Article

# Self-Assembled Donor Comprising Quantum Dots and Fluorescent Proteins for Long-Range Fluorescence Resonance Energy Transfer

Huachang Lu, Oliver Schps, Ulrike Woggon, and Christof M. Niemeyer

*J. Am. Chem. Soc.*, **2008**, 130 (14), 4815-4827 • DOI: 10.1021/ja078243f



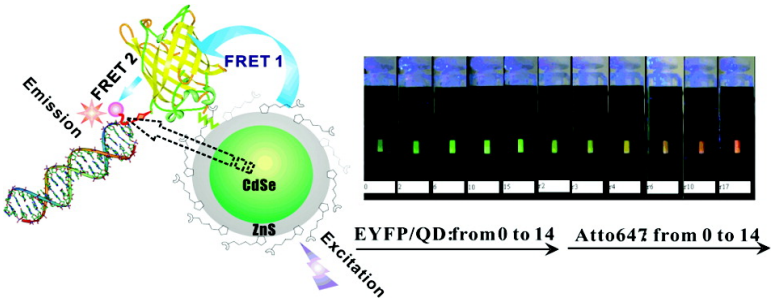


## More About This Article

Additional resources and features associated with this article are available within the HTML version:

- Supporting Information
- Links to the 1 articles that cite this article, as of the time of this article download
- Access to high resolution figures
- Links to articles and content related to this article
- Copyright permission to reproduce figures and/or text from this article

View the Full Text HTML

J|A|C|S
ARTICLES
Published on Web 03/14/2008

# Self-Assembled Donor Comprising Quantum Dots and Fluorescent Proteins for Long-Range Fluorescence Resonance Energy Transfer

Huachang Lu,[†] Oliver Schöps,[‡] Ulrike Woggon,*[,‡] and Christof M. Niemeyer*[,†]

*Technische Universität Dortmund, Fakultät Chemie, Biologisch-Chemische Mikrostrukturtechnik, Otto-Hahn Str. 6, D-44227 Dortmund, Germany, Technische Universität Dortmund, Fakultät Physik, Otto-Hahn Str. 4, D-44227 Dortmund, Germany*

Received October 28, 2007; E-mail: christof.niemeyer@tu-dortmund.de; ulrike.woggon@tu-dortmund.de

***Abstract:*** We report on the development of a self-assembled donor for long-range fluorescence resonance energy transfer (FRET). To this end, a three-chromophore FRET (3Ch−FRET) system was constructed, which consists of a luminescent quantum dot (QD), enhanced yellow fluorescent proteins (EYFP), and Atto647-dye-modified oligonucleotides. The system was assembled by electrostatic binding of covalent EYFP-ssDNA conjugate to the QD and subsequent hybridization with complementary oligonucleotides labeled with Atto647-dye. The final conjugates comprise three different two-chromophore FRET (2Ch−FRET) subsystems, QD/EYFP, QD/Atto647, and EYFP/Atto647, respectively, which were studied in detail by steady-state and time-resolved photoluminescence measurements. The helicity of DNA allowed us to control donor/acceptor separations and thus enabled the detailed analysis of the various FRET processes. We found that the 2Ch−FRET and the 3Ch−FRET (QD/EYFP/Atto647) systems revealed FRET efficiencies and transfer rates that were affected by the availability of distinct FRET pathways. The derived energy-transfer efficiencies and Förster radii indicated that within the 3Ch−FRET system, the 2Ch−FRET subsystem QD/EYFP showed highest FRET efficiencies ranging from 64 to 72%. Thus, it can be used as a powerful donor system that combines the intrinsic advantages of QDs (large and spectrally broad absorption cross section) and EYFP (high quantum yield) and enables long-distance FRET processes for donor−acceptor distances of up to 13 nm.

## Introduction

Fluorescence (or Förster) resonance energy transfer (FRET) is a process in which energy is transferred by a nonradiative, long-range dipole−dipole coupling from a fluorophore in an excited-state serving as a donor to another proximal ground-state acceptor. Because FRET usually occurs over distances realized in the interaction between most biomolecules, that is typically in the range of 1−10 nm, it is a powerful spectroscopic tool to interrogate changes in molecular conformation, association, and the assembly or disassembly of biomolecular machinery.[1,2] Luminescent semiconductor quantum dots (QDs) are inorganic nanoparticle fluorophores with unique optical and spectroscopic properties that make them excellent fluorescent labels for bioimaging, sensing, and diagnostics.[3−6] QDs possess a variety of advantages over conventional organic dyes, such as high quantum yields, excellent photo and chemical stability, and size-dependent, tunable absorption and emission.[7] This allows one to exploit them as donors and acceptors in energy-transfer studies. In recent years, numerous advances have been achieved in QD-based FRET investigations, regarding both fundamental theoretical analyses and biological applications, including the design of biosensors and the analysis of biomolecular conformation and interaction.[2,5,8−19] A limitation of FRET studies usually stems from the fact that it only permits

[†] Fakultät Chemie, Biologisch-Chemische Mikrostrukturtechnik.
[‡] Fakultät Physik.

(1) Lakowicz, J. R. *Principles of Fluorescence Spectroscopy*, 2nd ed.; Kluwer/Plenum: New York, 1999.
(2) Sapsford, K. E.; Berti, L.; Medintz, I. L. *Angew. Chem., Int. Ed.* **2006**, *45*, 4562−4588.
(3) Bruchez, M.; Moronne, M.; Gin, P.; Weiss, S.; Alivisatos, A. P. *Science* **1998**, *281*, 2013−2015.
(4) Chan, W. C. W.; Nie, S. M. *Science* **1998**, *281*, 2016−2018.
(5) Medintz, I. L.; Uyeda, H. T.; Goldmann, E. R.; Mattoussi, H. *Nat. Mater.* **2005**, *4*, 435−446.
(6) Michalet, X.; Pinaud, F. F.; Bentolila, L. A.; Tsay, J. M.; Doose, S.; Li, J. J.; Sundaresan, G.; Wu, A. M.; Gambhir, S. S.; Weiss, S. *Science* **2005**, *307*, 538−544.
(7) Woggon, U. Optical Properties of Semiconductor Quantum Dots. In *Springer Tracts in Modern Physics*, 1996; Vol. 136.
(8) Clapp, A. R.; Medintz, I. L.; Mattoussi, H. *ChemPhysChem* **2006**, *7*, 47−57.
(9) Willard, D. M.; Carillo, L. L.; Jung, J.; Van Orden, A. *Nano Lett.* **2001**, *1*, 469−474.
(10) Medintz, I. L.; Clapp, A. R.; Mattoussi, H.; Goldman, E. R.; Fisher, B.; Mauro, J. M. *Nat. Mater.* **2003**, *2*, 630−638.
(11) Clapp, A. R.; Medintz, I. L.; Mauro, J. M.; Fisher, B. R.; Bawendi, M. G.; Mattoussi, H. *J. Am Chem. Soc.* **2004**, *126*, 301−310.
(12) Kim, J. H.; Morikis, D.; Ozkan, M. *Sens. Actuators, B* **2004**, *102*, 315−319.
(13) Medintz, I. L.; Konnert, J. H.; Clapp, A. R.; Stanish, I.; Twigg, M. E.; Mattoussi, H.; Mauro, J. M.; Deschamps, J. R. *Proc. Nat. Acad. Sci. U.S.A.* **2004**, *101*, 9612−9617.
(14) Medintz, I. L.; Berti, L.; Pons, T.; Grimes, A. F.; English, D. S.; Alessandrini, A.; Facci, P.; Mattoussi, H. *Nano Lett.* **2007**, *7*, 1741−1748.
(15) Clapp, A. R.; Medintz, I. L.; Uyeda, H. T.; Fisher, B. R.; Goldman, E. R.; Bawendi, M. G.; Mattoussi, H. *J. Am. Chem. Soc.* **2005**, *127*, 18212−18221.
(16) Goldman, E. R.; Medintz, I. L.; Whitley, J. L.; Hayhurst, A.; Clapp, A. R.; Uyeda, H. T.; Deschamps, J. R.; Lassman, M. E.; Mattoussi, H. *J. Am. Chem. Soc.* **2005**, *127*, 6744−6751.

the analysis of interactions between two molecular entities. Many biochemical processes, however, involve multicomponent molecular assemblies, which are based on dynamic and highly coordinated supramolecular interactions. To study multimolecular interactions within, for instance biomolecular machineries, more complex FRET systems, in particular three-chromophore FRET systems, have been developed, which enable the analysis of up to three mutually dependent energy-transfer processes occurring between the fluorophores.[20−28] Other examples concern two-step FRET processes to achieve a higher efficiency in long-range energy transfer, larger spectral shifts between absorption and emission and improved sensitivity, compared to the simpler one-step FRET.[10,29] Thus, three-chromophor FRET (3Ch−FRET) systems are considered to possess a great potential for elucidating biomolecular structure and dynamics.

It has previously been suggested that the combination of different types of fluorophores, such as inorganic luminescent nanocrystals, organic dyes, and genetically encoded fluorescent proteins offers a promising route for the fabrication of multichromophore systems.[2] We here follow this notion and report on the assembly and spectroscopic characterization of a DNA-based 3Ch−FRET system. In contrast to previous work concerning binary fluorescent protein-based FRET systems,[30−32] we here employ three different types of fluorophores that are luminescent CdSe/ZnS quantum dots (QDs), enhanced yellow fluorescent protein (EYFP), and short single-stranded DNA (ssDNA) oligonucleotides tagged with the organic dye Atto647, all of which are common fluorescent tags in biolabeling and biosensing. In the self-assembled 3Ch−FRET systems, sketched as **4** in part A of Figure 1, the interchromophore distances can be changed by varying the binding sites of the fluorophores at the DNA carrier helix linked to the EYFP. The goal of our study was to understand of the various competitive FRET pathways, which can occur in **4** to estimate whether such systems might be applicable for exploiting long-distance FRET processes. One key goal was to assemble a highly efficient 2Ch−FRET subsystem consisting of QD and EYFP, which can function as a new donor in the 3Ch−FRET system. By taking advantage of the QD/EYFP 2Ch−FRET system, which combines the


(17) Medintz, I. L.; Clapp, A. R.; Brunel, F. M.; Tiefenbrunn, T.; Tetsuo Uyeda, H.; Chang, E. L.; Deschamps, J. R.; Dawson, P. E.; Mattoussi, H. *Nat. Mater.* **2006**, *5*, 581−589.
(18) Shi, L.; Rosenzweig, N.; Rosenzweig, Z. *Anal. Chem.* **2007**, *79*, 208−214.
(19) Shi, L.; De Paoli, V.; Rosenzweig, N.; Rosenzweig, Z. *J. Am. Chem. Soc.* **2006**, *128*, 10378−10379.
(20) Ramirez-Carrozzi, V. R.; Kerppola, T. K. *Proc. Natl. Acad. Sci. U.S.A.* **2001**, *98*, 4893−4898.
(21) Tong, A. K.; Li, Z. M.; Jones, G. S.; Russo, J. J.; Ju, J. Y. *Nat. Biotechnol.* **2001**, *19*, 756−759.
(22) Liu, J. W.; Lu, Y. *J. Am. Chem. Soc.* **2002**, *124*, 15208−15216.
(23) Haustein, E.; Jahnz, M.; Schwille, P. *ChemPhysChem* **2003**, *4*, 745−748.
(24) Watrob, H. M.; Pan, C. P.; Barkley, M. D. *J. Am. Chem. Soc.* **2003**, *125*, 7336−7343.
(25) Galperin, E.; Verkhusha, V.; Sorkin, A. *Nature Methods* **2004**, *1*, 209−217.
(26) Heilemann, M.; Tinnefeld, P.; Mosteiro, G. S.; Parajo, M. G.; Van Hulst, N. F.; Sauer, M. *J. Am. Chem. Soc.* **2004**, *126*, 6514−6515.
(27) Klostermeier, D.; Sears, P.; Wong, C. H.; Millar, D. P.; Williamson, J. R. *Nucleic Acids Res.* **2004**, *32*, 2707−2715.
(28) Lee, N. K.; Kapanidis, A. N.; Koh, H. R.; Korlann, Y.; Ho, S. O.; Kim, Y.; Gassman, N.; Kim, S. K.; Weiss, S. *Biophys. J.* **2007**, *92*, 303−312.
(29) Kawahara, S.-i.; Uchimaru, T.; Murata, S. *Chem. Commun.* **1999**, 563−564.
(30) Kukolka, F.; Mueller, B. K.; Paternoster, S.; Arndt, A.; Niemeyer, C. M.; Braeuchle, C.; Lamb, D. C. *Small* **2006**, *2*, 1083−1089.
(31) Kukolka, F.; Schoeps, O.; Woggon, U.; Niemeyer, C. M. *Bioconjugate Chem.* **2007**, *18*, 621 - 627.
(32) Hering, V. R.; Gibson, G.; Schumacher, R. I.; Faljoni-Alario, A.; Politi, M. J. *Bioconjugate Chem.* **2007**, *18*, 1705−1708.


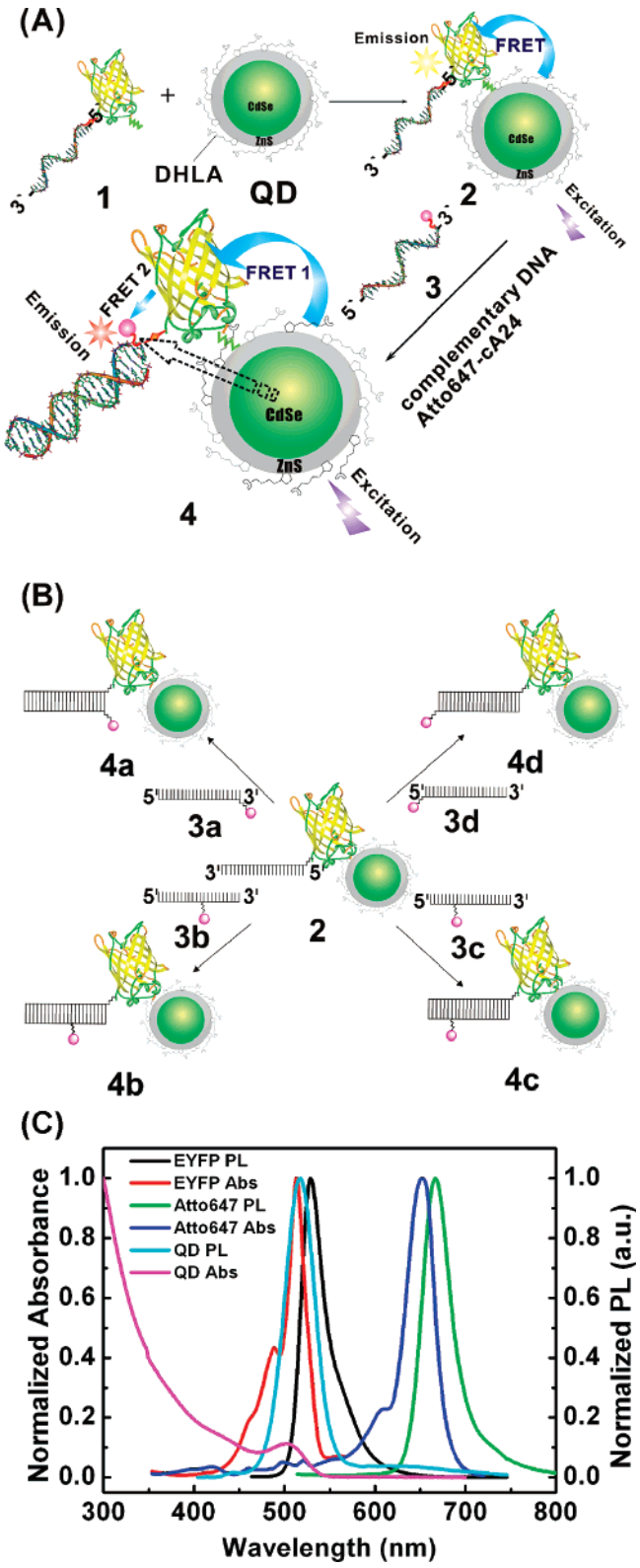


***Figure 1.*** Schematic representation and spectral properties of the DNA-based 3Ch−FRET system QD−EYFP−Atto647. (A) Initially, ssDNA− EYFP conjugates (termed as **1**) were adsorbed to DHLA-coated QDs to form QD−EYFP−A24 conjugate (**2**). **2** is hybridized with complementary Atto647-modified ssDNA (**3**) to form the final 3Ch−FRET conjugate (**4**); (B) four different DNA-based QD−EYFP−Atto647 conjugates (**4a**−**d**) were assembled using four different Atto647−cA24 oligonucleotides (**3a**−**d**) comprising the Atto647 dye at base pairs 0, 10, 17, or 24, respectively, counted from the 3′ end of **3**; (C) spectroscopic characterization of the DHLA−QDs' absorption (magenta) and emission (cyan), EYFP's absorption (red) and emission (black), and Atto647's absorption (blue) and emission (green).

advantages of QDs (large absorption cross section, tunable size, and spectral properties) with those of fluorescent proteins (high quantum yields), we were able to redirect the energy transfer from the QD directly to the Atto647 dye using the EYFP/Atto647 FRET channel. As a consequence of using QD/EYFP instead of EYFP or QD as the donor, long-distance FRET occurred within donor−acceptor distances of up to 13 nm with an efficiency of 5%, as compared to 0.3% obtained for using QD only.

The chemical synthesis and self-assembly of our 3Ch−FRET system is illustrated in Figure 1. We used ssDNA−EYFP conjugates (**1** in part A of Figure 1), which contained the 24-mer oligonucleotide A24, covalently linked to an engineered cysteine residue at the EYFP's C terminus, in addition to a hexahistidine tail at the N terminus.[33] Multiple conjugates of **1** were adsorbed on the surface of dihydrolipoic acid (DHLA)-coated QDs, thus leading to the formation of a two-chromophore FRET system (**2** in part A of Figure 1). The DNA−EYFP conjugates in **2** were then used for specific hybridization with complementary ssDNA labeled with the organic dye Atto647 (**3**) to yield the final supramolecular system (**4** in part A of Figure 1). Because of the modular design, four different FRET systems (**4a**−**4d** in part B of Figure 1) could be readily assembled by the hybridization of **2** with various complementary oligonucleotides, each of which contained the Atto647 dye coupled to a different nucleotide (**3a** through **3d** in part B of Figure 1), thus enabling us to gradually vary the donor−acceptor distances of the FRET systems.

In the course of this work, we initially characterized the three two-chromophore (2Ch−FRET) subsystems, that is, QD/EYFP, QD/Atto647, and EYFP/Atto647, using steady-state and time-resolved photoluminescence (PL) spectroscopy. Because the 2Ch−FRET system QD/EYFP exhibited spectrally strongly overlapping EYFP absorption and QD emission bands along with very close emission maxima of EYFP and QD (part C of Figure 1), FRET efficiencies were difficult to derive from standard titration experiments. Therefore, we combined several independent experimental approaches, that is, Gaussian fitting of photoluminescence, photoluminescence excitation spectroscopy (PLE), and rate equation simulations of time-resolved luminescence to measure and verify the energy-transfer rates and efficiencies of the QD/EYFP subsystems. Subsequently, the FRET efficiencies of the full systems (**4a**−**4d** in part B of Figure 1) were then derived and compared with the efficiency data deduced from the independent 2Ch−FRET subsystems. The transfer efficiencies of all of the FRET pairs can be translated into donor/acceptor distances by taking into account the respective Förster radii. The knowledge of these distances additionally allowed an estimation of the spatial arrangement of the multi-FRET constituents, which was compared to a geometric model taking into account the helicity of the DNA. Because this system, to the best of our knowledge, represents the first demonstration of a 3Ch−FRET system comprising QDs, fluorescent proteins, and dye-labeled DNA oligonucleotides, we anticipate that our results will open the door to further studies on the interaction of QDs and fluorescent proteins[34] as well as to the development of general tools for the investigation of multiprotein and protein−DNA assemblies.

(33) Kukolka, F.; Niemeyer, C. M. *Org. Biomol. Chem.* **2004**, *2*, 2203 - 2206.
(34) Geissbuehler, I.; Hovius, R.; Martinez, K. L.; Adrian, M.; Thampi, K. R.; Vogel, H. *Angew. Chem., Int. Ed.* **2005**, *44*, 1388−1392.

## Experimental Section

**Synthesis and Water-Solubilization of Luminescent QDs.** Semiconductor QD CdSe−ZnS were prepared using a high-temperature growth and annealing method of organometallic compounds as previously described.[35−37] The obtained CdSe−ZnS nanocrystals were rendered water-soluble by surface ligand exchange from the native hydrophobic trioctylphosphine oxide/trioctylphosphine TOPO/TOP ligands to dihydrolipoic acid (DHLA) using protocols previously reported.[38,39] The quantum yield of the resulting DHLA−QDs was estimated to 3.3% by comparing the integrated fluorescence intensity to that of rhodamine 6G in ethanol.[40] For FRET studies, QDs with an ensemble emission wavelength at ∼517 nm ($T$ = 300 K) were used, which corresponds to an average QD radius of around 2 nm.

**Synthesis of EYFP-DNA Conjugates.** The fluorescent protein EYFP (emission at 528 nm, extinction coefficient $\epsilon = 84\,000\ M^{-1}cm^{-1}$) was covalently coupled to the 5′ end of the 24-mer amino-modified single-stranded DNA (ssDNA) aA24 (sequence: 5′amino-TCC TGT GTG AAA TTG TTA TCC GCT-3′), yielding EYFP−A24 conjugate using a coupling strategy developed previously.[33] Briefly, an EYFP mutant was created by site-directed mutagenesis containing an extra cysteine residue at the C terminus, which is exposed on the protein's surface. The protein was expressed in *E. coli* and purified by $Ni^{2+}$-nitrilotriacetic acid chromatography. The 24-mer oligonucleotide containing an aliphatic primary amino group at the 5′ end was first activated with the heterobifunctional crosslinker sulfosuccinimidyl-4-[*N*-maleimidomethyl]-cyclohexane-1-carboxylate, which comprises a maleimide and an *N*-hydroxy-succinimide ester group that are reactive toward thiols and primary amines, respectively. The maleimide-containing DNA oligomers were puriefied by gel-filtration and subsequently coupled to the extra cystine residue on EYFP. The resulting DNA−EYFP conjugates (**1** in part A in Figure 1) were purified by anion-exchange chromatography and stored in 20 mM tris-buffered saline containing 150 mM NaCl, 5 mM EDTA, and 0.005% TWEEN-20, at pH 7.5 (TETBS buffer).

**Self-Assembly of QD/EYFP−A24 Conjugates.** The assembly of CdSe/ZnS QDs containing a hydrophilic monolayer of dihydrolipoic acid (DHLA) with DNA−EYFP conjugate **1** was performed similar to the approach reported by Mattoussi and colleagues, in which polyhistidine−labeled proteins or short peptides were attached to DHLA-capped QDs.[8,10,11,13,14,17,39] It is known that this immobilization occurs due to zinc−histidine coordination.[10,41] To assemble QD−EYFP−A24 donor−acceptor FRET conjugates (**2**, in part A of Figure 1), DHLA-capped QDs (0.1 $\mu$M solution in TETBS buffer) were mixed with solutions containing **1** (1.4 $\mu$M in TETBS buffer). Titration experiments revealed that the binding of **1** to the surface of DHLA−QDs due to the metal−histidine coordination mechanism occurred fast and was completed within a few minutes (Figure 2).

**Assembly of the 3Ch−FRET System QD/EYFP/Atto647.** Atto647-labeled oligonucleotides, Atto647−cA24 (emission at 667 nm, extinction coefficient $\epsilon = 120\,000\ M^{-1}cm^{-1}$) were purchased lyophilized from TIB MOLBIOL (Berlin, Germany), dissolved in $ddH_2O$ at a concentration of 100 $\mu$M, and stored at −20 °C until use. In these conjugates, the Atto647 fluorophore was attached either through a $C_6$-linker to the 3′ end (**3a**), through a $C_7$-linker to the 5′ end (**3d**), or

(35) Murray, C. B.; Norris, D. J.; Bawendi, M. G. *J. Am. Chem. Soc.* **1993**, *115*, 8706−8715.
(36) Peng, Z. A.; Peng, X. G. *J. Am. Chem. Soc.* **2001**, *123*, 183−184.
(37) Hines, M. A.; Guyot-Sionnest, P. *J. Phys. Chem.* **1996**, *100*, 468−471.
(38) Mattoussi, H.; Mauro, J. M.; Goldmann, E. R.; Anderson, G. P.; Sundar, V. C.; Mikulec, F. V.; Bawendi, M. G. *J. Am. Chem. Soc.* **2000**, *122*, 12142−12150.
(39) Clapp, A. R.; Goldman, E. R.; Mattoussi, H. *Nat. Protocols* **2006**, *1*, 1258−1266.
(40) Gussin, H. A.; Tomlinson, I. D.; Little, D. M.; Warnement, M. R.; Qian, H. H.; Rosenthal, S. J.; Pepperberg, D. R. *J. Am. Chem. Soc.* **2006**, *128*, 15701−15713.
(41) Flora, B.; Gusman, H.; Helmerhorst, E. J.; Troxler, R. F.; Oppenheim, F. G. *Protein Expression Purif.* **2001**, *23*, 198−206.

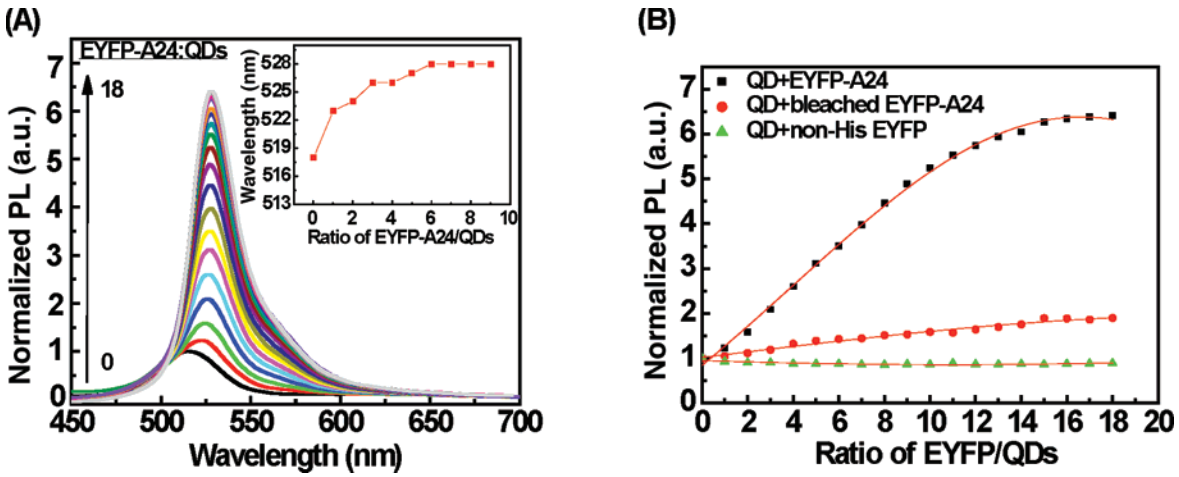


***Figure 2.*** PL evolution of the 2Ch−FRET subsystem QD/EYFP (conjugate **2** in part A of Figure 1). (A) Titration of QDs with increasing ratios of EYFP−A24 (**1**) measured at an excitation wavelength of 372 nm. The inset shows the shift of the PL maximum with increasing ratio of **1**; (B) PL enhancement as a function of the ratio **1**/QD (black squares); **1*/QD** (red dots) and the control experiment comprising QDs and non-histidine tagged EYFP (green triangles). Note that all data were corrected for the EYFP PL background and normalized against unconjugated QDs.

through a $C_2$-linker at two different thymine bases dT at the 10th (**3b**) and 17th (**3c**) base-pair positions from the 3′ end of the 24mer oligonucleotide cA24(5′-AGCGGATAACAATTT CACACAGGA-3′). The QD/EYFP−A24 conjugates **2** and the Atto647-labeled cA24 oligomers were assembled in a two-step process. In the first step, a titration was carried out by continuously adding 0.1−1.4 $\mu$M of conjugate **1** to 0.1 $\mu$M DHLA−QDs in TETBS solution until the saturation of the QDs surface was reached. This titration was followed by fluorescence spectroscopy (Figure 2), which indicated the formation of a supramolecular FRET complex comprising a spherical DHLA−QD and ∼14 EYFP−A24 conjugates. The resulting two-chromophore FRET system was further referred to as the QD/EYFP 2Ch−FRET subsystem. In the second step, the three-chromophore FRET system was assembled by hybridizing Atto647-labeled cA24 oligomers (**3a-d**) to the EYFP−A24 conjugates attached at the QDs surface. This led to the formation of the four 3Ch−FRET systems (**4a-d**, respectively, in Figure 1B) with varying donor−acceptor distances between Atto647 and the EYFP luminescent center. In TETBS buffer solutions of the final 3Ch−FRET systems, the concentrations of QDs, EYFP−A24, and Atto647−cA24 were approximately 0.1, 1.4, 1.4 $\mu$M, respectively. Additional 2Ch−FRET subsystems, EYFP−A24/Atto647, were assembled by hybridization of EYFP−A24 conjugate **1** with the four Atto647-labeled oligonucleotides **3a**−**d**.

**EYFP−A24 Conjugate Bleaching and Assembly of QD/Atto647 Subsystems.** To enable determination of direct FRET from the QDs to the Atto647, additional 2Ch−FRET subsystems (denoted as QD/Atto647) were assembled using photobleached EYFP−A24 conjugates to connect the two components. The bleached EYFP−A24 conjugates were also used for the investigation of the unaffected interaction of QD/EYFP. To this end, EYFP−A24 conjugate **1** in TETBS buffer was irradiated using an argon laser with an intensity of 50 mW at the wavelength of 514 nm (EYFP absorbance maximum) at room temperature for ∼6−8 h. As determined by fluorescence and UV/vis absorbance spectroscopy, this treatment led a ∼99% decrease in the EYFP's PL (part A in Figure S1 in the Supporting Information). The resulting EYFP−A24 species, denoted as **1***, was used for the conjugation with DHLA−QDs to form the QD−protein conjugate **2***. The latter (**2***) was used in fluorescence titration experiments to analyze the increase in QDs PL upon binding to hexahistidine-tagged proteins (red dotted line in part b of Figure 2). The 2Ch−FRET QD/Atto647 subsystems, denoted as **4a*** to **4d***, were assembled using bleached EYFP−A24 **1*** by mixing 14 molar equiv of **1*** with DHLA−QDs to generate conjugate **2***. The latter was allowed to hybridize with 14 molar equiv of the Atto647-labeled oligomers **3a**−**d** (Figure 4).

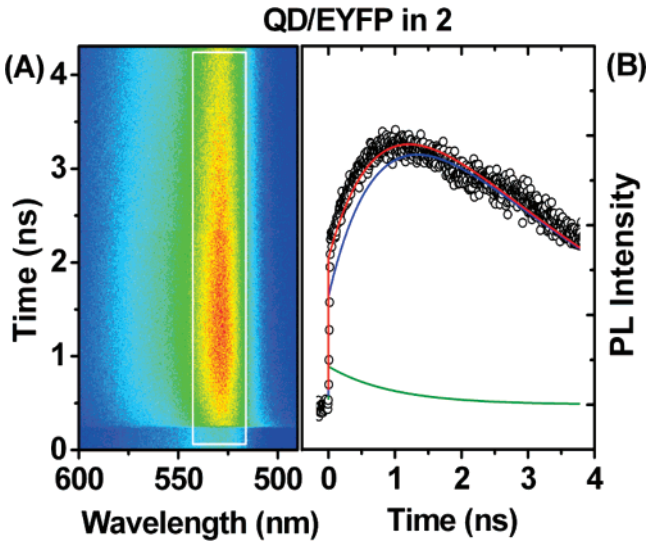


***Figure 3.*** Temporal evolution of the PL signal of the 2Ch−FRET subsystem QD/EYFP (**2**). (A) Spectrally and temporally resolved dynamics of the conjugate emission. The region over which the intensity was spectrally integrated to generate the cut, shown in the right panel, is indicated by the white box. (B) Emission dynamics of the spectrally integrated QD/EYFP conjugate (black dots). The red curve shows the simulated overall intensity of the two-chromophore system with the parts contributed by the QDs (green) and the EYFP (blue). The simulated results were obtained using the parameters for QD (EYFP): molar concentration 1 (14); QY 0.066 (0.62); radiative decay rate, 0.019 $ns^{-1}$ (0.20 $ns^{-1}$); transfer rate QD to EYFP, 0.053 $ns^{-1}$.

**UV−vis, Photoluminescence (PL), and 2D-PLE Measurements.** PL spectra were recorded with a CARY-Eclipse fluorescent spectrophotometer (Varian, Austria), and UV−vis spectroscopic measurements were carried out using a 100 Bio UV−vis spectrophotometer (Varian, Austria). All of the spectroscopic data were taken at room temperature. The excitation wavelength of the 3Ch−FRET systems was chosen at 372 nm, where the QDs absorb strongly, whereas both EYFP and Atto647 display minimal absorption. For the monitoring of the PL intensity as a function of detection and excitation wavelength in photoluminescence excitation spectroscopy (PLE), a 150 W xenon lamp attached to a 1 m monochromator was used as a tuneable excitation source. The excitation wavelength was scanned with a step size of 1 nm, whereas the excitation intensity at that wavelength was measured

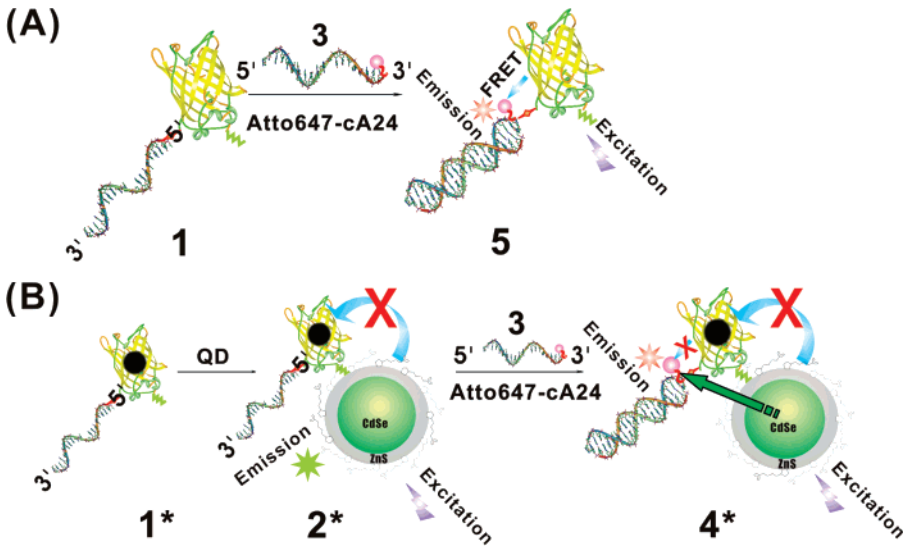


***Figure 4.*** Schematic representation of the 2Ch−FRET subsystems EYFP/Atto647 and QD/Atto647. (A) Assembly of the EYFP/Atto647 subsystem (**5**) by hybridization of EYFP−A24 (**1**) with cA24−Atto647 (**3**). (B) Assembly of the QD/Atto647 subsystem (**4***) comprising photobleached EYFP−A24 (**1***) as the bridge in between the QD and Atto647-labeled oligonucleotides.

with a photodiode. The sample's luminescence was recorded with a TE-cooled CCD camera attached to a 0.85 m imaging spectrometer, resulting in a spectral resolution of 0.4 nm. The acquired spectra were background corrected and normalized to the exciting photon flux recorded simultaneously. The resulting intensities were displayed as a color coded 2D-PLE plot with detection wavelength and excitation wavelength as the x and y axes, respectively.

**Time-Resolved PL Measurements.** Solutions of samples (typically 1.0−1.4 $\mu$M in TETBS buffer) in a UV transparent cuvette were illuminated by the frequency-doubled output of a Ti:Sapphire laser, resulting in 1 mW at 374 nm with a repetition rate of 75.4 MHz and a pulse width of about 150 fs. The luminescence was collected with an achromatic lens, after which scattered excitation light was filtered out by a long-pass filter. The PL signal was fed to the entrance slit of a 0.46 m imaging spectrometer with a spectral resolution of 2 nm. The output spectrum was temporally dispersed and recorded using a Hamamatsu streak camera, with a time-resolution of 20 ps. This yielded a 2D representation of the PL as a function of emission wavelength and time.

## Results and Discussions

**Energy Transfer Processes in the Two-Chromophore FRET Subsystems.** Prior to elucidation of the 3Ch−FRET system QD/EYFP/Atto647, we initially characterized the less complex 2Ch−FRET subsystems, namely QD/EYFP, QD/Atto647, and EYFP/Atto647. The quantitative study of these FRET pairs required the knowledge of distinct parameters, such as the Förster radius or energy-transfer rates. For the 2Ch−FRET systems QD/EYFP and QD/Atto647, where a single exciton donor can interact with several acceptors and the energy-transfer efficiency depends on the molar ratio of the acceptor and donor. $E$ can be expressed as

$$E(N,r) = \frac{N}{N + \left(\frac{r}{R_0}\right)^6} \qquad (1)$$

where $N$ is the average number of acceptor molecules EYFP−A24 or Atto647 per one QD donor.[1,11] In the QD/EYFP and QD/Atto647 systems, $N = 14$ was chosen to ensure high FRET efficiency but keeping the number of acceptors below the observed saturation value of $N_{sat} = \sim 16$ (below). Because conjugate **1** contains only one DNA oligomer per EYFP,[33] $N = 1$ was chosen in the EYFP/Atto647 subsystem. The Förster radius $R_0$, defined as the distance between the donor and acceptor that yields 50% energy-transfer efficiency, can be calculated as[1]

$$R_0^{\,6} = 8.8 \times 10^{23} \kappa_p^{\,2} n_D^{\,-4} Q_D J \qquad (2)$$

where $Q_D$ is the quantum yield (QY) of the donor in the absence of an acceptor, $n_D$ is the refractive index of the medium, and $\kappa_p^2$ is an orientation factor, depending on the relative orientation of the donor and acceptor dipoles. $\kappa_p^2 = {}^2/_3$ is the value for randomly oriented dipoles, which is suited for the systems studied here.[17] The overlap integral $J$ is a quantitative measure of donor−acceptor spectral overlap integrated over all wavelengths $\lambda$, and is defined as[1]

$$J = \int f_D(\lambda)\epsilon_A(\lambda)\lambda^4 d\lambda \qquad (3)$$

where $f_D$ and $\epsilon_A$ represent the donor emission spectrum (normalized and dimensionless) and acceptor absorption spectrum, respectively. Using eq 3, the overlap integrals of the three 2Ch−FRET subsystems QD/EYFP, QD/Atto647, and EYFP/Atto647 were calculated with the help of the software *PhotoChemCAD*,[42] and they are listed in Table 1.

Experimentally, the efficiency $E$ of a FRET process can, for example, be derived from the quenching of the donor fluorescence intensity, according to[1]

$$E = 1 - \frac{F_{DA}}{F_D} = 1 - \frac{\tau_{D-A}}{\tau_D} = \frac{k_{transfer}}{k_{rad} + k_{nonrad} + k_{transfer}} \qquad (4)$$

where $F_D$ and $F_{DA}$ are the fluorescence intensities of the donor in the absence and presence of an acceptor, $\tau_{D-A}$ and $\tau_D$ are the fluorescent lifetimes of the donor in the absence and presence

(42) Du, H.; Fuh, R. C. A.; Li, J. Z.; Corkan, L. A.; Lindsey, J. S. *Photochem. Photobiol.* **1998**, *68*, 141−142.

***Table 1.*** Measured Efficiencies *E*, Calculated Overlap Integrals *J*, Förster Radii $R_0$, Donor−Acceptor Distances *r*, and Structurally Estimated Donor−Acceptor Distance for the Three 2Ch−FRET Subsystems **2**, **5a**−**d**, and **4a***−**d***

| donor–acceptor pair | overlap integral, $J \times 10^{-14}$ cm$^3$M$^{-1}$ | Förster radius, $R_0$ (nm) | efficiency | D–A distance, *r* from *E* (nm)[a] | D–A distance, *r* from structural estimate (nm) |
|---|---|---|---|---|---|
| QD/EYFP in **2** | 29.4 | 3.86 | 0.72 ± 0.02 | 5.11 ± 0.06 | 5.1 |
| EYFP/Atto647 in **5a** | 8.00 | 4.83 | 0.78 ± 0.02 | 3.91 ± 0.08 | 4.2 |
| EYFP/Atto647 in **5b** | | | 0.43 ± 0.02 | 5.06 ± 0.07 | 5.4 |
| EYFP/Atto647 in **5c** | | | 0.23 ± 0.03 | 5.91 ± 0.16 | 6.3 |
| EYFP/Atto647 in **5d** | | | 0.072 ± 0.02 | 7.40 ± 0.44 | 8.3 |
| QD/Atto647 in **4a**[c] | 8.80 | 3.16 | 0.31 ± 0.02[b] | 5.61 ± 0.09 | 4.5 |
| QD/Atto647 in **4a**[c] | | | 0.12 ± 0.02 | 6.84 ± 0.20 | 7.4 |
| QD/Atto647 in **4a**[c] | | | 0.028 ± 0.001 | 8.86 ± 0.05 | 9.3 |
| QD/Atto647 in **4a**[c] | | | 0.003 ± 0.002 | 12.9 ± 1.1 | 12.1 |

[a] Estimated using $r = R_0*(N(1 - E)/E)^{1/6}$, where $N = 14$ for the QD−Atto647 and QD/EYFP pair and $N = 1$ for the EYFP/Atto647 pair. [b] The efficiencies of four different QD/Atto647 pairs were obtained from acceptor PL gain. [c] Bleached EYFP−A24 (**1***) was used for assembly.

of an acceptor, and $k_{rad}$, $k_{nonrad}$, and $k_{transfer}$ are the radiative and nonradiative recombination rates and the transfer rate of the donor, respectively. Alternatively, the efficiency *E* can be determined by the acceptor fluorescence enhancement (if the acceptor is a fluorescent molecule), expressed as[43]

$$E = \frac{A_A(\lambda_D)}{A_D(\lambda_D)}\left[\frac{F_{AD}(\lambda_A)}{F_A(\lambda_A)} - 1\right] \quad (5)$$

where $\lambda_D$ is the donor excitation wavelength, $A_D$ and $A_A$ are the donor and acceptor absorbance at the wavelength $\lambda_D$, and $F_{AD}$ and $F_A$ are acceptor fluorescent intensities at the acceptor emission wavelength $\lambda_A$ in the presence and absence of a donor. The efficiencies *E* of the four different 2Ch−FRET subsystems QD/Atto647 were calculated from acceptor PL gain. The efficiency *E* of the QD/EYFP and four EYFP/Atto647 subsystems were obtained from donor PL quenching. All of the efficiency data were verified by combining several experimental methods, in particular, 2D-PLE, time-resolved luminescence and titration results.

**1. QD/EYFP 2Ch−FRET Subsystem.** A peculiarity of the QD/EYFP FRET pair is its large spectral overlap between the QD donor emission and the EYFP acceptor absorption, which is reflected by a large overlap integral *J* (Table 1). Whereas such strong overlap is necessary to yield highly efficient energy transfer, the PL quenching of the QDs is difficult to extract due to the spectral overlap of the QD and EYFP emission (part C of Figure 1). To analyze the FRET process, we therefore carried out three independent experiments: (i) titration of QDs with an increasing number of EYFP−A24 conjugates per QD, (ii) comparison titration of QD with photobleached EYFP−A24* conjugates (i.e., QD/**1***) (Figure 2), and (iii) measurement of the PL dynamics and modeling of the energy-transfer rates using rate equation systems (Figure 3 and Supporting Information). As outlined below, all three methods led to similar and thus consistent results.

The results of the titration experiments are shown in Figure 2. The coverage of the QD surface with EYFP molecules can theoretically be estimated by the expression,[38]

$$N_{EYFP-A24} = 0.65\left(\frac{(R_2^3 - R_1^3)}{R_p^3}\right) \quad (6)$$

where $R_1$ is the core−shell spherical nanocrystal radius (without the DHLA cap) and $R_2 \sim R_1 + 2R_p$ is the radius of the QD plus bound EYFP−A24 molecules. In this model, the protein molecules are assumed to be close-packed spheres around the central QD. Being a mutant of *aequorea* GFP, EYFP also has a so-called $\beta$-barrel structure with a diameter of ∼2.3−3.0 nm and a length of ∼4.0−4.2 nm, similar to that of GFP.[44] Comparative titration experiments, carried out with EYFP and EYFP-24 (**1**), showed that saturation occurred at approximately 13−16 molar equiv of protein per QD and this was very similar for EYFP and EYFP−A24 (see also Figure S2 in the Supporting Information). This result is in good agreement with a theoretical estimation of surface loading, using values of $R_p = \sim 2.1$ nm (half length of EYFP), $R_1 = \sim 2.0$ nm for the CdSe/ZnS QD with an emission of 517 nm (estimated from CdSe absorption data and the ZnS thickness), and the filling factor of 0.65 for eq 6, leading to $N_{EYFP-A24} = \sim 16$ per QD. The titration experiments of QD/EYFP and QD/EYFP−A24 also indicated that PL enhancement was significantly greater in the case of QD/EYFP as compared to QD/EYFP−A24 (Figure S2 in the Supporting Information). The reasons for this observation are currently unclear. However, one may speculate that the increased polarity of the EYFP−A24 might lead to a less efficient hydrophobic shielding of the QDs surfaces, as compared to the pure EYFP.

Part A of Figure 2 shows the PL evolution of the 2Ch−FRET subsystem QD/EYFP with increasing EYFP/QD ratio. To clarify changes in the spectral properties of the QD/EYFP system, disturbing emission from directly excited EYFP was subtracted using PL spectra measured from samples containing similar concentrations of EYFP−A24 (**1**). In addition, the fluorescence intensity results are all normalized with respect to the fluorescence intensity of unconjugated QDs (for original data, see Figure S3 in the Supporting Information). It was evident from part A of Figure 2 that the adsorption of **1** to the QD led to an increase in PL emission. Moreover, a significant red-shift of the emission peak from ∼517 to ∼528 nm was observed (inset of part A of Figure 2), suggesting an energy transfer from the QD donor to the EYFP acceptors. To verify that these spectral changes, indeed, were due to FRET processes, we carried out control experiments using a non-hexahistidine tagged EYFP. It is shown in part B of Figure 2 (green triangles) that this titration led to only negligible enhancement in fluorescence and no shift

(43) van der Meer, B. W.; Coker, G.; Chen, S.-Y. S. *Resonance Energy Transfer: Theory and Data*; Wiley-VCH: New York, 1994.

(44) Yang, F.; Moss, L. G.; Phillips, G. N., Jr. *Nat. Biotechnol.* **1996**, *14*, 1246−1251.

of the emission peak, as compared to the results obtained with the hexahistidine-tagged EYFP (black squares). Thus, the experiments supported our hypothesis that the binding of EYFP to the surface of QDs led to a Förster energy transfer from QD to **1**. The FRET efficiency $E$ of this QD/EYFP 2Ch−FRET subsystem was calculated using eq 4, using the intensity of the QD emission extracted from the total PL spectrum by Gaussian fits. The latter were used because the spectral overlap of the emission spectra of EYFP and QD brings with it difficulties for data analysis. We therefore used Gaussian fitting based on the narrow and symmetric QD emission properties, which allowed us to extract the QD emission spectra from the overlap. This approach enabled the reproduction of the PL shape with high accuracy. We reasoned that the QD PL emission in the absence of acceptors should be equal to the emission obtained from the QD-bleached EYFP−A24 conjugates (**2***), because **2*** comprises the modification of the QD-quantum yield (here a PL enhancement) due to shielding of negatively charged DHLA−QDs by the adsorbed positively charged protein domains (i.e., polyhistidine). The photobleaching strategy provides a nonfluorescent species for control experiments such as the study of QD PL enhancement effect due to QD−protein interaction and the FRET study of QD/Atto647 subsystems described below. Taking into account this PL enhancement effect, we obtained a high FRET efficiency of $E = \sim 0.72 \pm 0.02$, suggesting that, as a result of very efficient FRET, the QD/EYFP 2Ch−FRET subsystem should act as a new, combined-donor complex within the anticipated 3Ch−FRET system.

To confirm the calculated number of $E = \sim 0.72$, the temporal evolution of the 2Ch−FRET subsystem QD/EYFP was investigated by time-resolved fluorescence spectroscopy (Figure 3). To this end, samples containing the QD/EYFP conjugates were excited with pulsed laser light of the same wavelength used in the aforementioned time-integrated PL experiments. As indicated from Figure 3, the QD/EYFP system's emission qualitatively showed an increase in intensity, which reached its maximum at approximately 1 ns after the arrival of the exciting laser pulse. This can be explained by the energy transferred from the QD to the EYFP because the decrease of the QD PL is accelerated, whereas the EYFP emission gains intensity until the feeding reservoir of the QD is depleted. For comparison, the PL decay of a sample comprising QDs and photobleached EYFP (**2***) was measured and found to display a fast initial decay in the first 100 ps, before a monoexponential decay with a time constant of $\tau = \sim 3.5$ ns becomes visible. This decay time and the measured quantum yield of 6.6% translate into a radiative decay rate of 0.019 $ns^{-1}$. For a more quantitative analysis, the emission was spectrally binned over a wavelength range around the maximum of combined QD/EYFP emission, centered at 528 nm to produce an intensity versus time plot representation. The fraction of the total QD emission present in this region, as well as the corresponding value for the EYFP, were extracted from time-integrated measurements. For the numerical simulation of the energy-transfer rates, the following channels of population and depopulation have been taken into account: The QD is excited by the laser and releases the energy via radiative recombination, nonradiative recombination, and transfer to the EYFP. The protein is excited by the laser as well, though to a much smaller extent due to the absorption cross section at the chosen excitation wavelength of 372 nm. Additionally, the transferred energy from the QD donor populates this excited-state of the acceptor, which is depopulated by radiative and nonradiative channels. Rates represent the strength of the respective energy migration channels and allowed us to calculate excitations present in the QD and the EYFP in an iterative way (Supporting Information). The simulated results were obtained with the following parameters for QD and (EYFP), respectively: molar ratio, 1 (14); QY, 0.066 (0.62); radiative decay rate, 0.019 $ns^{-1}$ (0.20 $ns^{-1}$); and transfer rate of QD to EYFP of 0.053 $ns^{-1}$. These FRET transfer rates are consistent with the FRET efficiency value $E$ obtained from the titration experiments. The excellent match with the observed dynamics confirmed the high FRET efficiency in the 2Ch−FRET subsystem QD/EYFP.

According to eq 1, a FRET efficiency of $E = \sim 0.72$ results in a distance of $r = \sim 5.11 \pm 0.06$ nm between the QD center and the EYFP center, taking into account a Förster radius of $R_0 = 3.86$ nm for the QD/EYFP 2Ch−FRET subsystem (Table 1). This value for $r$ is in good agreement with the estimate from geometrical considerations that take into account the size of the QD, the dimension and shape of EYFP, and the interaction between these two fluorophores. The QD is attached to the barrel-shaped EYFP molecule through its N-terminal hexahistidine residue, which should position the QD into the region underneath the barrel bottom. Considering the 3D structure of EYFP, the distance between the centers of the QD and EYFP can be estimated by adding half of the diagonal length of the EYFP barrel (∼2.4 nm), the QD radius (∼2.0 nm), and the length of the hexahistidine tail (about 0.7 nm when all polyhistidine residues are coordinated to the QD surface[13]). This yields a value of $r = \sim 5.1$ nm, which nicely correlates with the value obtained from experimental data.

**2. EYFP/Atto647-2Ch−FRET Subsystem.** We continued our study by investigation the two Atto647-containing 2Ch−FRET subsystems, schematically depicted in parts A and B of Figure 4, following the strategy proposed by us.[31] The resulting data of the isolated EYFP/Atto647 system, that is, conjugates **5a**−**d**, comprising different separation distances between the two fluorophores, are listed in Table 1. The data clearly indicate the expected decrease in transfer efficiency upon increased donor−acceptor distances.

**3. QD/Atto647-2Ch−FRET Subsystem.** In contrast to the aforementioned studies on the 2Ch−FRET subsystems QD/EYFP and EYFP/Atto647, which were performed on the actual binary FRET systems, it was necessary to analyze the direct energy transfer between QD and the Atto647-labeled oligonucleotides using the ternary complex comprised of QD, EYFP, and Atto647. To facilitate direct QD-to-Atto647 energy transfer, we used photobleached, and thus dark, EYFP−A24 (**1***), which was prepared by prolonged irradiation with an argon laser. Because of the nonfluorescent state of **1***, the FRET channel from QD to EYFP and from EYFP to Atto647 is blocked, thereby directing the energy tranfer from the QD directly to Atto647 in this 2Ch−FRET subsystem (**4***). This allowed us to explore the influences of chromophore separation distance on FRET processes occurring in the respective conjugates **4a***−**4d*** (Figure 5).

The energy-transfer efficiencies of the four 2Ch−FRET subsystems **4a***−**4d*** were derived from the changes in the emission spectra measured for **4a***−**4d*** with respect to a

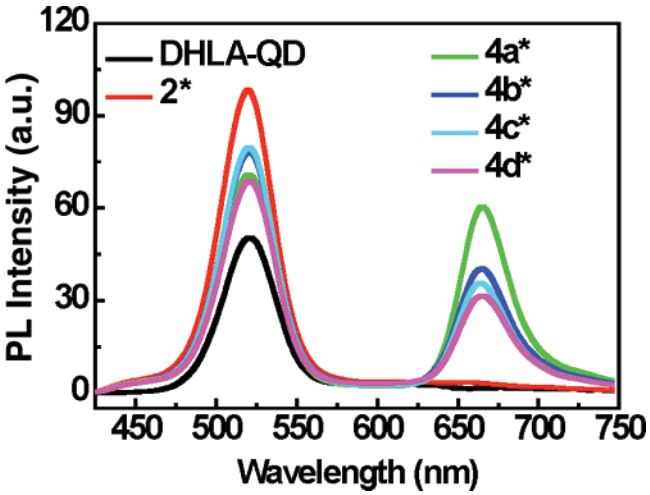


***Figure 5.*** PL spectra of the four different QD/Atto647 2Ch−FRET subsystems **4a***, **4b***, **4c***, and **4d***. The QD emission is centered at ∼520 nm and the Atto647 PL signal at 667 nm. The additional curves indicate the spectra obtained for DHLA−QDs only (black) and QDs to which photobleached EYFP−A24 (**1***) was adsorbed (red). The excitation wavelength was 372 nm.

reference spectrum obtained from QDs, which were saturated with photobleached EYFP (**2***). Conjugate **2*** was chosen because the protein coating of the QDs led to an approximately 2-fold enhancement in QD PL (above). The transfer efficiency was calculated both from the quenching of the QD PL (eq 4) and the PL gain of the Atto647 (eq 5) obtained from Figure 5. The observed quenching of QD PL in conjugates **4*** confirmed the direct FRET form QD to the Atto647-labeled oligomer. On the basis of QD quenching, an efficiency of ∼0.32 ± 0.02 was calculated for conjugate **4a***. For comparison, an efficiency of ∼0.31 ± 0.02 was obtained when the gain of the Atto647 emission was used for calculation. The latter method was also used to calculate FRET efficiencies occurring in conjugates **4b***−**4d***. All of the values obtained are listed in Table 1. They clearly indicate the expected dependence of FRET efficiency from the donor−acceptor distance, as realized in **4a***−**4d***. We then used the efficiency data to calculate the separation distances between the QD center and the Atto647 dye, leading to distances of ∼5.61 ± 0.09, 6.84 ± 0.20, 8.86 ± 0.05, and 12.9 ± 1.1 nm for **4a***−**4d***, respectively.

**4. FRET Parameters of the 2Ch−FRET Subsystems.** Because of their lower complexity, the three 2Ch−FRET subsystems investigated were well analyzable, and the results suggested that they form a suitable basis of the intended three-chromophore FRET system. The various efficiencies $E$, calculated overlap integrals $J$, Förster radii $R_0$, donor−acceptor distances $r$, and the structurally estimated donor−acceptor distance of the three 2Ch−FRET subsystems, **2** (QD/EYFP−A24), **5a**−**d** (EYFP−A24/cA24−Atto647), and **4a***−**d*** (QD/EYFP−A24/cA24−Atto647 containing photobleached EYFP) are summarized in Table 1. The results obtained for **2** confirmed the expected high FRET efficiency of $E = 0.72$, which is most likely due to the existence of 14 parallel QD-to-EYFP transfer channels, all of which exhibit the high value of the overlap integral $J$, which compensates for the small quantum yield QY of the DHLA-capped QDs (in contrast to the high QY of the EYFP). The other two 2Ch−FRET systems exhibited similar spectral overlap intergrals, however, slightly different Förster radii of 4.83 nm (EYFP/Atto647) and 3.16 nm (QD/Atto647). Because of the relatively low QY of the DHLA-capped QD used here and the larger separation between chromophores, the QD/Atto647 subsystem revealed significantly smaller but not negligible FRET efficiencies. It was therefore interesting to see whether this latter transfer acts as a competitive side channel in the three-chromophore FRET system as well, or whether its relative contribution is decreased due to the presence of the stronger parallel transfer occurring from QD/EYFP to the Atto647.

**Energy Transfer Processes in the Three-Chromophore FRET.** The 3Ch−FRET system, as depicted in Figure 1, comprises the combination of two competitive FRET channels, namely, that from QD to Atto647 and that from QD to EYFP to Atto647, which will be modified, and finally controlled, in their individual weightings in the total FRET process. For the quantitative characterization of the strength of an energy-transfer channel, two representations are common. The use of the transfer rate, which can be interpreted as the probability of an excitation being transferred within a given time interval, is a measure of the absolute magnitude of energy transfer. The transfer efficiency, which is easily connected to measured quantities, weights the energy-transfer channel with respect to all other present channels of energy loss. The two complementary representations are connected via eq 7.

$$E = 1 - \frac{F_{DA}}{F_D} = 1 - \frac{\tau_{D-A}}{\tau_D} = \frac{k_{transfer1}}{k_{rad} + k_{nonrad} + k_{transfer1} + k_{transfer2}} \quad (7)$$

In the efficiency representation, the presence or absence of a competitive energy-transfer channel can change the efficiency value, even if the original strength of transfer given by the transfer rate is not altered. In this way, efficiencies can be tailored by offering alternative pathways of energy migration.

From the assembly point of view, preformed QD−EYFP−A24 conjugates **2** were allowed to hybridize with 14 molar equiv of the Atto647-labeled complementary oligonucleotide **3** to yield the ternary target conjugates **4a**−**d**. The alternative strategy, that is, to add to a solution containing QDs, 14 equiv of preformed EYFP−DNA−Atto647 (**5**) led to identical effects in PL (data not shown), thus suggesting that the self-assembly of the three components, indeed, occurred as expected. The constitution of target conjugates **4a**−**d** is similar to that of the 2Ch−FRET subsystem **4a***−**d*** because the bleaching of EYFP (in **4***) only damages the chromophore center but not the protein's conformation;[45,46] we assumed that the QD/EYFP, EYFP/Atto647 and QD/Atto647 donor−acceptor separation distances within **4** are the similar to those estimated from the respective two-chromophore subsystems listed in Table 1.

We continued to unravel the pathways of energy migration in **4** by comparing the energy-transfer efficiencies derived from the measurements of **4** with those obtained from the systems possessing only a single transfer channel (**2**, **4***, and **5**). It is to

(45) Swaminathan, R.; Hoang, C. P.; Verkman, A. S. *Biophys. J.* **1997**, *72*, 1900−1907.
(46) Tsien, R. Y. *Annu. Rev. Biochem.* **1998**, *67*, 509−544.

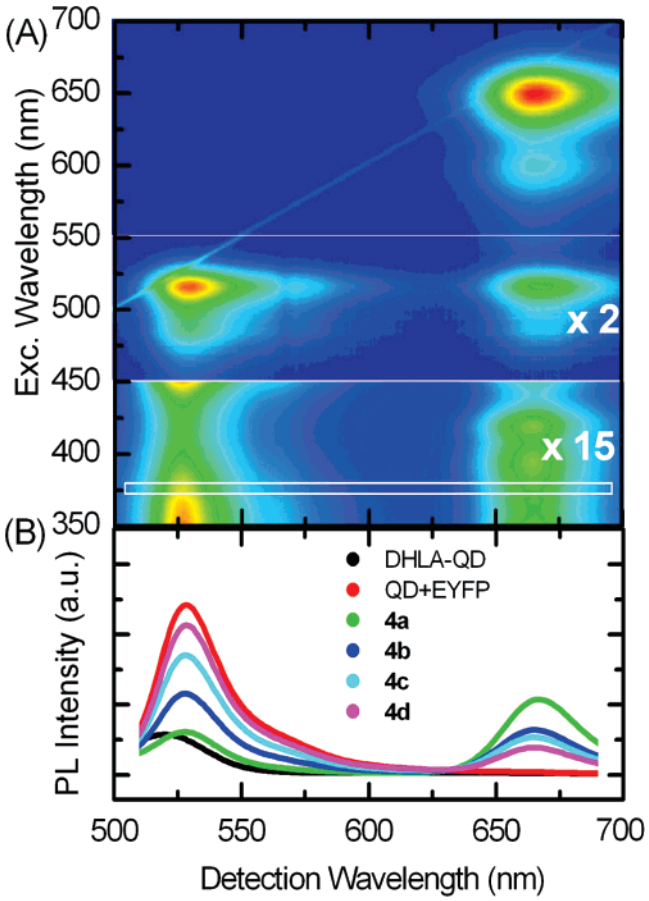


***Figure 6.*** (A) Full excitation−emission characteristics of 3Ch−FRET systems, as exampled by 2D-PLE analysis of system **4b**. Excitation wavelengths longer than 550 nm show the directly excited Atto647 emission. The 450 to 550 nm part (enhanced 2-fold) shows the transfer from the QD/EYFP subsystem to Atto647. The bottom part (enhanced 15×) shows direct Atto647 excitation, QD−Atto647 transfer, and the sequential QD−EYFP−Atto647 transfer. (B) Changes of the PL intensity at an excitation wavelength of 372 nm (white box in part A of Figure 6) as a function of acceptor presence: DHLA−QD, QD/EYFP (**2**), and FRET systems **4a**−**d.**

be expected that the efficiency of the EYFP to Atto647 transfer remains unchanged because neither the distances nor spectral overlap or other parameters influencing the energy transfer are changed. The opening of an additional depopulation channel for the QD, by allowing it to transfer energy not only to the EYFP, but also directly to the Atto647 dye, however, should influence the values for the transfer efficiency. This can be seen most clearly from the definition of transfer efficiencies as a function of the transfer rates *k*, as indicated in eq 4. The radiative and nonradiative rates are those defining the QDs' intrinsic quantum yield, and, therefore, they should be constant in all of the assemblies investigated. Whereas the transfer rate is simply the QD-to-EYFP transition rate in system **2**, and the QD-to-Atto647 transition rate in system **4***, it needs to be understood as the sum of the QD-to-EYFP and the direct QD-to-Atto647 rates in the 3Ch−FRET system.

**FRET Parameters of the 3Ch−FRET System Derived from PL and 2-PLE Data.** Figure 6 shows an overview of the donor−acceptor emission spectra measured for the four 3Ch−FRET systems **4a**−**d**. Part A of Figure 6 shows a map of the emission measured by so-called 2D photoluminescence, on the exemplary 3Ch−FRET system **4b** (for the full 3Ch−FRET system, **4a**−**d**, see Figure S4 in the Supporting Information). In part B of Figure 6, the PL spectra are plotted for the four 3Ch−FRET systems **4a**−**d** as well as for the reference systems QD only and QD/EYFP (conjugate **2**), all excited at 372 nm. To explore possible spectral dependencies of the FRET efficiencies caused by quantum-confinement induced spectral modifications in the QD-absorption cross section, we initially mapped the emission characteristics as a function of excitation wavelength (2D-PLE) over a broader spectral window, as illustrated in Figure 6A. The excitation wavelength was tuned from short excitation wavelengths/high energies (350 nm/3.54 eV) toward longer wavelengths/lower energies (700 nm/1.77 eV) in steps of 1 nm while recording for each excitation the corresponding emission spectrum within a detection range between 500 and 700 nm. Excitation wavelengths longer than 550 nm show the directly excited Atto647 emission. The 450 to 550 nm part (enhanced 2-fold) shows the transfer from the QD/EYFP subsystem to Atto647. The bottom part (enhanced 15×) shows direct Atto647 excitation, QD−Atto647 transfer, and the sequential QD−EYFP−Atto647 transfer. FRET processes were evidenced in the 2D-PLE of part A of Figure 6 by the off-diagonal transfer peak. This appeared as PL intensity at the spectral position of the acceptor's recombination wavelength, whereas the system was excited at wavelengths of strong donor absorption.[31] In contrast to an organic dye or a fluorescent protein, where the luminescence is excited within a narrow band, the semiconducting nature of QDs provides well-defined electron hole pair states within the QD. The resonance energy of the states is modified by the confinement potential, which is directly related to the size. Consequently, the size distribution within the QD ensemble smears out the sharp absorption peaks and produces the well-known absorption spectrum as shown in part C of Figure 1. It is the simultaneous mapping of a whole emission wavelength range as a function of excitation wavelength, which enables the determination of spectral windows, suited for the analysis of the FRET subsystems. The spectral region from 450 to 520 nm exhibits QD absorption, but the onset of the absorption of the EYFP prohibits the observation of the QD-to-Atto647 transfer. The analysis of the FRET pathways from QD to Atto647, therefore, has to focus on the excitation in the wavelength range of 350 to 400 nm, which is shown, 15-fold magnified, in the lower spectral window in part A of Figure 6. At an excitation wavelength of 372 nm, the transfer signature is strong and not concealed by emission stemming from direct excitation of the Atto647, whereas the EYFP absorption is negligible (see also Supporting Information for the PLE maps of the systems **4a**−**d**). We therefore limited our quantitative analysis of energy-transfer efficiencies to the selected excitation wavelength of 372 nm (part B of Figure 6).

The FRET efficiency data can be obtained from part B of Figure 6 or following a study presented by Watrob and colleagues for a similar multicomponent FRET system.[24] According to this study, the efficiencies and Förster radii of different FRET pairs in 3Ch−FRET system **4** can be derived from the results of the 2Ch−FRET subsystems (QD/EYFP, QD/Atto647, and EYFP/Atto647 pairs of conjugates **2**, **5**, and **4***; Table 1) using the following formulas, which were generated from the kinetic calculations for the energy-transfer

***Table 2.*** Efficiency $E$, Förster Radius $R_0$ for 3Ch−FRET Systems **4a**−**d,** Derived from the 2Ch−FRET Subsystems (QD/EYFP, QD/Atto647 and EYFP/Atto647 Pairs of Conjugate **2**, **5**, and **4***) and Corresponding Donor−Acceptor Separation Distances $r$

| donor−acceptor pair | efficiency derived from independent system data [a] | Förster radius, $R_0$ (nm) | D–A distance $r$ (nm)[b] |
|---|---|---|---|
| QD/EYFP in **4a** | 0.64 ± 0.02 | 3.63 | 5.11 ± 0.06 |
| QD/EYFP in **4b** | 0.69 ± 0.02 | 3.78 | |
| QD/EYFP in **4c** | 0.71 ± 0.02 | 3.84 | |
| QD/EYFP in **4d** | 0.72 ± 0.02 | 3.86 | |
| QD/Atto in **4a** | 0.11 ± 0.02 | 2.55 | 5.61 ± 0.09 |
| QD/Atto in **4b** | 0.037 ± 0.007 | 2.56 | 6.84 ± 0.20 |
| QD/Atto in **4c** | 0.008 ± 0.001 | 2.56 | 8.86 ± 0.05 |
| QD/Atto in **4d** | 0.001 ± 0.001 | 2.63 | 12.9 ± 1.1 |
| EYFP/Atto647 in **4a** | 0.78 ± 0.02 | 4.83 | 3.91 ± 0.08 |
| EYFP/Atto647 in **4b** | 0.43 ± 0.02 | | 5.06 ± 0.07 |
| EYFP/Atto647 in **4c** | 0.23 ± 0.03 | | 5.91 ± 0.16 |
| EYFP/Atto647 in **4d** | 0.072 ± 0.02 | | 7.40 ± 0.44 |

[a] Based on eqs 8 and 9. [b] $r$ of all of the FRET pairs, equal to the 2Ch−FRET subsystems due to maintained configurations.

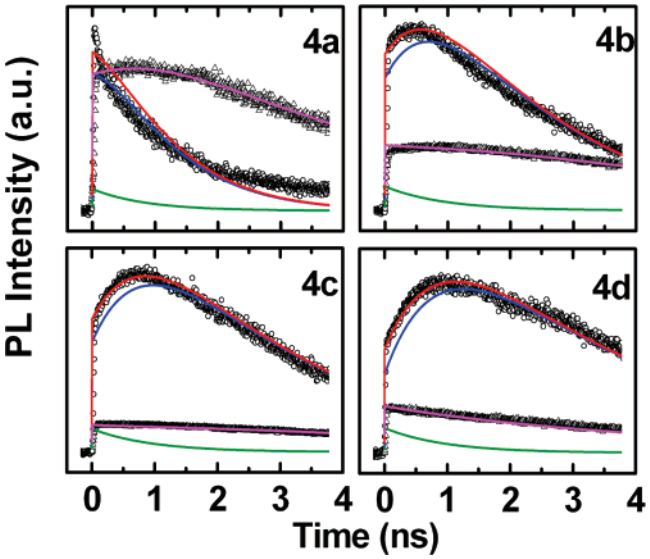


***Figure 7.*** Temporal evolution of the spectrally resolved luminescence signal of the four FRET systems **4a**−**d** and their simulated behavior. The data points show the intensity recorded in the wavelength range of QD and EYFP emission (circles) and at the Atto647 emission wavelength (triangles). The simulated curves display the dynamics of QD (green), EYFP (blue), the sum of QD and EYFP (red), and Atto647 (magenta).

rates in a three-chromophore system[24,25]

$$E'_{QA} = \frac{E_{QA} - E_{QA} \times E_{QE}}{1 - E_{QA} \times E_{QE}} \quad (8)$$

$$E'_{QE} = \frac{E_{QE} - E_{QE} \times E_{QA}}{1 - E_{QE} \times E_{QA}} \quad (9)$$

where $E'_{QA}$ and $E'_{QE}$ are the FRET efficiency of QD → Atto647 and QD → EYFP in the 3Ch−FRET system **4** (**4a**−**4d**), and $E_{QA}$ and $E_{QE}$ are the corresponding ones of the 2Ch−FRET subsystems **2** and **4*** (**4a***−**4d***). The results of the efficiency calculations are listed in Table 2.

The effect of the additional transfer channel is most readily visible on the example of system **4a**. Whereas the QD-to-EYFP and the QD-to-Atto647 transfer efficiencies were ∼0.72 and ∼0.31 respectively in the systems displaying only a single transfer channel (**2** and **4a***, respectively), these values were reduced to ∼0.64 and ∼0.11 respectively when both channels were open simultaneously, as calculated by eqs 8 and 9. This decrease in FRET efficiency between QD and EYFP can be interpreted as the result of the competition between two pathways for FRET from the QD toward two different acceptors in the 3Ch−FRET system. In a complementary way, the decrease of the FRET efficiency from QD to Atto647 in conjugate **4a** compared with **4a*** (from ∼0.31 to ∼0.11) is due to the same competition between parallel energy-transfer mechanisms. Consequently, the reduced efficiency of a transfer in the presence of a competitive acceptor can be specified by recalculating the characteristic Förster radii $R_0$, which are no longer constant when exposing a donor species to two acceptors. This representation was chosen for the listing in Table 2.

Using the one-step FRET efficiency data $E'_{QE}$, $E'_{QA}$, and $E_{EA}$ of conjugate **4**, two kinds of overall FRET efficiencies for the 3Ch−FRET system can be derived based on the following equation system.[24,25]

$$E_{QA}^{TOT} = E_{QA}^{SEQ'} + E'_{QA} = E'_{QE} \times E_{EA} + E'_{QA} \quad (10)$$

$$E_{Q\rightarrow EA}^{THEOR} = E'_{QE} + E'_{QA} \quad (11)$$

where $E'_{QE}$, $E'_{QA}$, and $E_{EA}$ are the corresponding one-step FRET efficiencies for the conjugates **4** (**4a**−**4d**). Equation 10 demonstrates the total efficiency from the QD to Atto647 (the entire energy transferred to the Atto647 dye), which represents the parallel efficiency with one of the parts reflecting the sequential FRET efficiency. Experimentally, this efficiency can be measured by comparing the acceptor Atto647 emission gain at the presence and absence of the donor based on eq 5 from the data shown in part B of Figure 6. Equation 11 represents the theoretical combined efficiency from QD to both EYFP and Atto647 acceptors (the entire energy transferred away from the QD). Likewise, this efficiency can be obtained experimentally from the quenching of the QD emission signal based on eq 4. The total efficiency from the QD to the Atto647 dye of ∼0.61 ± 0.02, 0.33 ± 0.02, 0.17 ± 0.02, and 0.052 ± 0.02 for conjugates **4a**, **4b**, **4c** and **4d**, respectively, agree well with the experimental data obtained from the Atto647 signal enhancement: ∼0.58 ± 0.04, 0.30 ± 0.06, 0.16 ± 0.02, and 0.048 ± 0.02, respectively. The direct QD-to-Atto647 FRET ($E_{QA}'$ = ∼0.11, 0.037, 0.008, and 0.001) contributes 18, 10, 4, and 0.3% of the total energy transferred from QD to Atto647. The majority of ∼82, 90, 96, and 99.7% is contributed from the QD → EYFP → Atto647 FRET process. The efficiencies of combined energy transferred away from the QD to both EYFP and Atto647 were also calculated following eq 11. Good agreement with the values obtained experimentally from the QD quenching in the four constructs (**4a**−**4d**) was observed (errors of less than ∼3%, Table 3). These small errors substantiate the assumption we raised above that in all of the 3Ch−FRET systems QD/EYFP/Atto647 (**4a**−**d**) the spatial deviations of the chromophore orientations and distances are very small compared to those within 2Ch−FRET subsystems **2**, **4***, and **5**. Both the theoretically estimated and experimentally determined overall efficiencies calculated from the results shown in part B of Figure 6 for the 3Ch−FRET systems **4a**−**d** are listed in Table 3.

**FRET Parameter of the 3Ch−FRET System Derived from the Temporal Evolution of the Emission.** To further support

***Table 3.*** Two Types of Overall FRET Efficiency Derived from Independent FRET Data and Experimental Estimate of Two Types of Overall FRET Efficiency Obtained from Spectral Analysis of Conjugates 3Ch−FRET Systems **4a**−**d**

| 3Ch-FRET system | calculated combined efficiency from QD ($E_{Q\rightarrow E,A}$)[a] | measured combined efficiency from QD ($E_{Q\rightarrow E,A}$)[b] | calculated total efficiency transferred to Atto647 ($E_{Q,E\rightarrow A}$)[c] | measured total efficiency transferred to Atto647 ($E_{Q,E\rightarrow A}$)[d] |
|---|---|---|---|---|
| **4a** | 0.75 ± 0.02 | 0.74 ± 0.01 | 0.61 ± 0.02 | 0.58 ± 0.04 |
| **4b** | 0.73 ± 0.02 | 0.72 ± 0.02 | 0.33 ± 0.02 | 0.30 ± 0.06 |
| **4c** | 0.72 ± 0.02 | 0.73 ± 0.02 | 0.17 ± 0.02 | 0.16 ± 0.02 |
| **4d** | 0.72 ± 0.02 | 0.74 ± 0.03 | 0.053 ± 0.02 | 0.048 ± 0.02 |

[a] Calculated combined FRET efficiency of the energy-transfer process from the QD to both EYFP and Atto647, using eq 11. [b] Measured combined efficiency from QD to both EYFP and Atto647, derived from eq 4. [c] Calculated total FRET efficiency of all energy-transfer process to the Atto647, using eq 10. [d] Measured total efficiency of all of the energy-transfer process to the Atto647, derived from eq 5.

the FRET efficiencies obtained from the time-integrated experiments, the luminescence of the four multi-FRET samples **4a**−**4d** was recorded time-resolved and the decay curves were compared to the results of a numerical simulation as demonstrated in Figure 7. The evolution of the combined luminescence of the QD and the EYFP is accessible by binning the wavelength range from 521 to 547 nm of the temporally and spectrally dispersed luminescence signal to obtain a time versus intensity plot. Likewise, the decay of the Atto647 dye is accessible by extraction of the PL signal between 653 and 679 nm. The model calculation, which is an extension of the routines used to simulate the behavior in the QD/EYFP system explained above, takes into account the radiative and nonradiative recombination channels of the QD, the EYFP, and the Atto647 dye. Crosslinking channels are the transfer from the QD to the EYFP, the direct QD−Atto647 transfer, and the EYFP to Atto647 channel. Again the population of each subspecies is calculated in an iterative way with a simulated temporal resolution of 1 ps (Supporting Information for details of the simulation). The radiative recombination rates were extracted from fluorescence-lifetime measurements of the QDs, the EYFP, and the Atto647 dye, and their respective quantum yields. The transfer transition rates were then adjusted to match the efficiencies derived from time-integrated measurements. The result of such a simulation is compared to the measured PL of the system in Figure 7. The parameters used to obtain a consistent agreement are for the QD: QY = 0.066, $k_{rad}$ = 0.019 ns$^{-1}$; EYFP QY = 0.62, $k_{rad}$ = 0.2 ns$^{-1}$; and for the dye, Atto647 $k_{rad}$ = 0.05 ns$^{-1}$ and $k_{QD\rightarrow EYFP}$ = 0.053 ns$^{-1}$. The varying transfer rates in the four differently spaced multi-FRET systems are $k_{EYFP\rightarrow Atto}$ = 1.15 ns$^{-1}$, 0.245 ns$^{-1}$, 0.10 ns$^{-1}$, and 0.031 ns$^{-1}$; and $k_{QD\rightarrow Atto}$ = 0.0095 ns$^{-1}$, 0.0028 ns$^{-1}$, 0.0006 ns$^{-1}$, and 0.00008 ns$^{-1}$ for samples **4a**−**d**, respectively. It is striking, that at the closest proximity of the Atto647 dye to the EYFP (**4a**), when the energy is transferred to the dye most efficiently, the formation of the rise in the EYFP PL intensity is prevented, whereas the Atto647 displays a gain in emission (Figure 7). At larger distances, the characteristic behavior of the QD/EYFP system is recovered (also Figure 3), whereas the Atto647 emission is returning to the monoexponential behavior, which is also observed when the dye is not subject to energy transfer. In Table 4, we summarized the obtained radiative decay rates $k_{rad}$ and energy-transfer rates $k$ derived from the time-resolved emission of the four 3Ch−FRET systems **4a**−**d**.

According to the data listed in Table 2, the internal transfer from QD to EYFP in the four conjugates **4a**−**d** ranged from $E$ = ∼0.64 to $E$ = ∼0.72, indicating that the QD/EYFP−A24 conjugate **2** indeed acts as a combined donor complex. In addition to this high transfer efficiency, this donor complex benefits from the unique advantages of QD and fluorescent proteins and also overcomes the limitations of the individual components. The QD/EYFP−A24 conjugate with a large absorption cross section (from QD) and a high quantum yield (from EYFP) can be excited at a much broader wavelength region, and a more efficient transfer can be achieved. The QD also serves as a nanoscaffolding to assemble multiple EYFP−A24 species into a single complex, which to some extent integrates energy-transfer emitters. The oligonucleotide attached to the EYFP provides a functional coupling bridge for different acceptors, thus enabling the precise control over donor−acceptor separation distances. The donor emission center of the new complex is shifted from the QD center to the EYFP center and overcomes the inherent large size limitation of QDs, which also helps to achieve a long-range FRET. As an example, a donor−acceptor separation distance of ∼8.86 nm is achieved with a decent total FRET efficiency of ∼0.17 in conjugate **4c**, compared to a separation distance of only ∼5.91 nm in the respective conjugate **5c**, comprising only EYFP and Atto647 (Tables 1 and 2). A maximum separation distance of ∼12.9 nm could be reached in our case, which can hardly be achieved by a simple, two-chromophore FRET system.

***Table 4.*** Radiative Decay Rates $k_{rad}$ and Energy Transfer Rates $k$ Derived from the Time-Resolved Emission for the Four FRET Systems **4a**, **4b**, **4c**, and **4d** as Parts of the 3Ch−FRET System QD−EYFP−Atto647

| system | $k_{QD,rad}$ | $k_{EYFP,rad}$ | $k_{QD\rightarrow EYFP}$ | $k_{Atto647,rad}$ | $k_{QD\rightarrow Atto647}$ | $k_{EYFP\rightarrow Atto647}$ |
|---|---|---|---|---|---|---|
| **2** | | | | | | |
| **4a** | | | | | 0.0095 ns$^{-1}$ | 1.15 ns$^{-1}$ |
| **4b** | 0.019 ns$^{-1}$ | 0.2 ns$^{-1}$ | 0.053 ns$^{-1}$ | 0.05 ns$^{-1}$ | 0.0028 ns$^{-1}$ | 0.245 ns$^{-1}$ |
| **4c** | | | | | 0.0006 ns$^{-1}$ | 0.10 ns$^{-1}$ |
| **4d** | | | | | 0.00008 ns$^{-1}$ | 0.031 ns$^{-1}$ |

**Structural Arrangement of Components in the 3Ch−FRET System.** Whereas the distinct relation between transfer efficiency and distance in a single Förster-type energy transfer allows the calculation of the separations between the donor and the acceptor, the simultaneous presence of multiple FRET mechanisms allowed for insights into the spatial arrangement of the system's components. This is due to the fact that three distances between three points in space define their respective coordinates.

Picking up the aforementioned picture of the QD being attached to the barrel bottom of the EYFP, and taking into account that the DNA is attached to the same region of the C terminus of the protein, one can assume that the protein is being tilted to provide space for the flexible sulfo−SMCC linkage to the DNA. Knowledge of the transfer efficiency in the case of sample **4d**, which translates into a distance of 12.9 nm, strongly suggests that the flexible EYFP/DNA link is bent in a way that

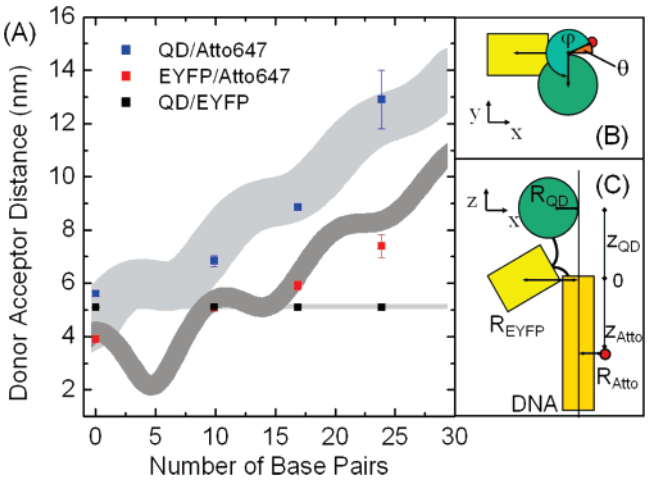


***Figure 8.*** (A) Donor/acceptor distances between QD, EYFP, and Atto647 derived from the measured transfer efficiencies. The gray regions indicate the results of according distance calculations with the parameters $R_{QD}$ = 2.5 nm, $R_{EYFP}$ = 2.8 nm, $R_{Atto}$ = 1.4 nm, $z_{QD}$ = −3.5 nm, and $\varphi$ = 270° based on a least-square fit to the data. The DNA helicity, furthermore, dictates $z_{Atto} = N \times 0.34$ nm and $\theta = N \times 36°$ with $N$ being the number of base pairs. (B) The cylindrical coordinate system, used to describe the positions of the multi-FRET constituents seen from top. The $z$ axis corresponds to the central DNA axis. The angular coordinate for the QD is $\varphi$ and for the Atto647 dye $\theta$. (C) Side view of the same coordinate system. The radial coordinates $R_{QD}$, $R_{EYFP}$ , and $R_{Atto}$ represent the distances from the $z$ axis. For simplicity, only one of the 14 EYFP/Atto647 conjugates is shown.

allows the DNA and the attached Atto647 dye to point away from the QD because this is the only configuration that allows for such a large QD/Atto647 separation while maintaining the QD/EYFP and the EYFP/Atto647 distances.

The EYFP/QD subsystem displays an energy-transfer efficiency that can be probed with high precision, thus allowing for a realistic estimation of a distance of 5.1 nm. The DNA helix of the EYFP/Atto647 subsystem provides well-defined values for the distance along, and the angle around, the DNA axis. However, the aliphatic linker molecules in between EYFP and DNA or Atto647 introduce uncertainties because they are rather long and flexible. The number of possible configurations and orientations is increased even further because the EYFP/Atto647 conjugates are likely bound flexible to the QDs surface. However, one can expect that the high loading of the QD surface ($N$ = ∼14) reduces the range of possible configurations. We therefore propose a geometric model of the 3Ch−FRET systems, which is based on the helicity of the DNA,[31,47] the rough knowledge of size and shape of the constituents and linkers, and especially on the measured transfer efficiencies to describe the structural properties of this multi-FRET system. Because the persistence length of DNA is about 50 nm, we estimated the short dsDNA as a rigid linker, although the aliphatic spacers in between DNA and both EYFP and QD should be considered flexible.

We had previously established that DNA maintains its double-helical B configuration in the EYFP−A24 conjugates,[31] and thus one can consider the DNA helix as a cylinder with the center of the top lid as the origin of a cylindrical coordinate system. The positions of the FRET constituents are being described by the parameters sketched in parts B and C in Figure 8. Starting at the origin, the EYFP position can be defined to be at a distance of $R_{EYFP}$ along the negative $x$ axis. The Atto647 position in the case of 0 base pairs between the two is fixed at a distance $R_{Atto647}$ in positive $x$ direction. With growing number of base pairs between these two chromophores, the Atto647 orbits the central DNA axis with an angle $\theta = N \times {}^{\pi}/_{5}$ and simultaneously descends along the $z$ axis as $z_{Atto} = N \times 0.34$ nm, with $N$ indicating the number of base pairs. This assumes that two base pairs are separated by 0.34 nm and that the DNA completes one revolution after the 10th base pair. The position of the QD can be represented by a respective set of coordinates $z_{QD}$, $\theta$, and $R_{QD}$. Simple geometric considerations were used to calculate the distances between the three multi-FRET constituents to compare them to those derived from the measured FRET efficiencies. The outcome of this spectroscopic triangulation is shown in part A of Figure 8. Taking into account the uncertainties mentioned above, we chose to display the calculated distances as a broad band reflecting estimated errors of 1.3, 0.5, and 0.1 nm in the calculation of the QD/Atto647, the EYFP/Atto647, and the QD/EYFP distances, respectively. The parameters used were: $R_{QD}$ = 2.5 nm, $R_{EYFP}$ = 2.8 nm, $R_{Atto647}$ = 1.4 nm, $z_{QD}$ = −3.5 nm, and $\varphi$ = 270°, and are based on a least-square fit to the data. Indeed, this simulation supported our hypothesis that the proteins are tilted on the QD surface to allow the DNA to place the Atto647 dye at a maximum possible distance from the QD. This assumption is further corroborated by the fact that the DNA only marginally changes the effective size of the EYFP, derived from of the maximum number of proteins on the QD surface, which was demonstrated in the analysis of the QD/EYFP 2Ch−FRET subsystem (Figure S2 in the Supporting Information).

## Conclusions

We here described the detailed analysis of a novel supramolecular energy-transfer system, comprised of inorganic luminescent QD, the fluorescent protein EYFP, and DNA oligonucleotides labeled with the organic dye Atto647. The QDs function both as the nanoscaffold to facilitate self-assembly of the system as well as the primary donor for energy transfer to the fluorescent proteins. This binary system essentially works as a novel donor for efficient long-range energy transfer to the Atto647, the latter of which is positioned at distinct distances by means of the double-helical DNA spacer. Spatial configurations such as relative orientations, donor−acceptor separation distances, Förster radii, and transfer efficiencies of each of the three implemented QD/EYFP, QD/Atto647, and EYFP/Atto647 2Ch−FRET pairs were elucidated by both theoretical and experimental approaches and found to be consistent. Fluorescent lifetime measurements of QD/EYFP and QD/EYFP/Atto647 systems provided additional proof of the FRET processes occurring between the three chromophores. As a novel approach to investigate interactions between luminescent QD and fluorescent proteins, we here employed photobleaching to unambiguously measure the PL enhancement caused by the adsorption of proteins to the QD and to allow one to take into account this change in QDs' spectral properties to elucidate transfer processes.

We here observed that, in the 3Ch−FRET system, a dominant QD → EYFP → Atto647 FRET pathway largely overrules the direct QD → Atto647 FRET path. This is caused by the fact that, in the 3Ch−FRET system, the 2Ch−FRET subsystem QD/

(47) Clegg, R. M.; Murchie, A. I.; Zechel, A.; Lilley, D. M. *Proc. Natl. Acad. Sci. U.S.A.* **1993**, *90*, 2994−2998.

EYFP, comprised of QDs containing up to 14 molecules of EYFP, showed the highest FRET efficiencies, ranging from 64 to 72%. Thus, the 2Ch−FRET QD/EYFP subsystem functions as a powerful donor, which combines the intrinsic advantages of QDs (large and spectrally broad absorption cross section) with the high quantum yields of EYFP, thereby enabling long-distance FRET processes over 9−13 nm with efficiencies of 17−5%, respectively. The efficiency values are significantly higher than those of the direct QD-to-Atto647 transfer (0.8−0.1%, respectively) thereby impressively demonstrating the power of the self-assembled QD/EYFP donor. These results, in particular, suggest that supramolecular donors assembled from QDs and fluorescent proteins may enable for long-range FRET detection in a variety of applications, such as FRET-based high-throughput screening assay or in vivo observation of spatial and temporal regulation of signaling processes.

**Acknowledgment.** We thank Florian Kukolka and Binil Itty Ipe for helpful discussions. H.C.L and C.M.N. acknowledge the International Max Planck Research School on Chemical Biology for a fellowship and the Zentrum für Angewandte Chemische Genomik (ZACG) for financial support.

**Supporting Information Available:** Detailed information on the bleaching of EYFP−A24, titration comparison for QD/EYFP and QD/EYFP−A24, raw data for PL evolution of conjugates **2** and QD/non-histagged EYFP, the description of the simulation model for time-resolved data analysis, and the full 2D-PLE data for **4a** to **4d** systems. This material is available free of charge via the Internet at http://pubs.acs.org.

JA078243F